Supplementary Information

Surface-Fixed Mechanochemical Refinement for Nanoscale Lithium Superionic Conductors

Jeongbin Son[1,2#], Seong Min Lee[3,#], Do Woon Yoon[1], Su-Bin Ki[3], Min Wook Pin[3], Sanghyeon Park[4], Jinyoung Chun[1], Kwang Chul Roh[1], Dae Soo Jung[1], Chan-Woo Lee[5], Jong Min Yuk[4], Yeon Sik Jung[4], Jungjae Park[3,*], and Kyeong Min Song[1,*]

#These authors contribute equally to this work.

[*] Email address: jungjae10@rist.re.kr (J.Park), kmsong@kicet.re.kr (K.M.Song)

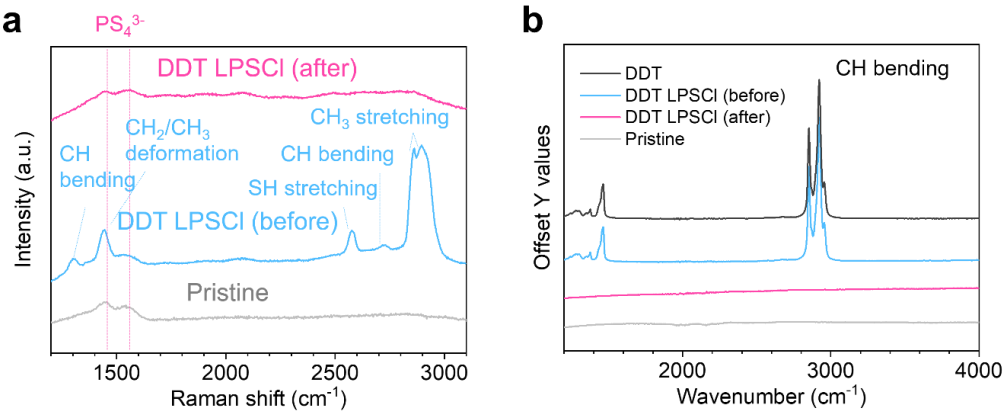

Supplementary Fig. 1 | Spectroscopic validation of temporary surfactant coordination and complete ligand removal. a, Raman spectra of pristine LPSCl solid Li-ion conductor, DDT-assisted milled LPSCl before thermal treatment, and DDT-assisted milled LPSCl after mild thermal annealing. The pristine sample displays the characteristic PS_4^{3-} tetrahedral symmetric stretching mode at 425 cm^{-1}. Before thermal treatment, the spectrum of the hybrid sample exhibits distinct vibrational peaks corresponding to the dodecanethiol (DDT) ligand: CH bending at ~ 1300 cm^{-1}, CH_2/CH_3 deformation at 1440 cm^{-1}, an additional CH bending mode at 1465 cm^{-1}, S-H stretching from the thiol head group at 2575 cm^{-1}, and CH_3/CH_2 stretching bands from the alkyl tail in the range of $2850–2960 cm^{-1}. Following the mild thermal treatment, all organic-related peaks disappear, leaving only the native PS_4^{3-} framework peak, which demonstrates complete volatilization of the ligand. **b,** Fourier-transform infrared (FTIR) spectra of the solid electrolyte samples across the same processing states. Prior to thermal annealing, a distinct CH bending vibration associated with the hydrocarbon tail of DDT is observed at 1460 cm^{-1}. After the thermal treatment, this organic absorption band is completely eliminated, yielding a spectrum identical to that of pristine LPSCl, confirming that the surfactant layer leaves no carbonaceous residue on the solid Li-ion conductor surface.

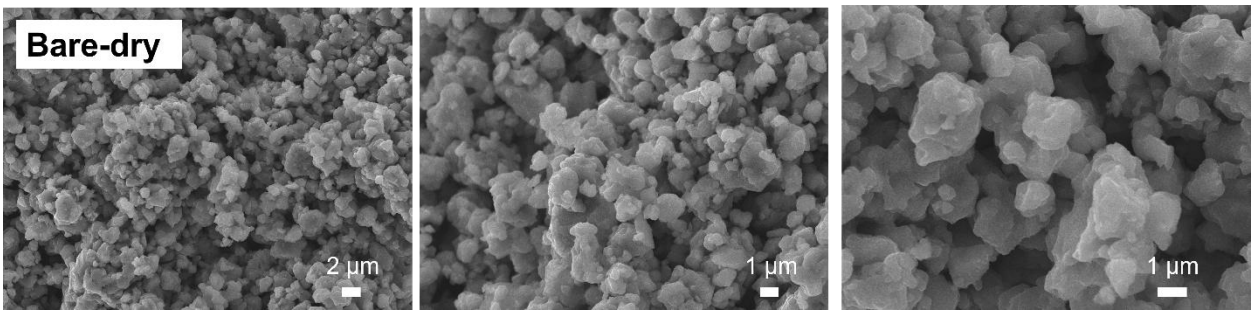

Supplementary Fig. 2 | Scanning electron microscopy (SEM) images of bare dry-milled solid electrolyte. Representative SEM micrographs of LPSCl particles obtained after conventional dry ball-milling without additives, displayed at multiple magnifications to illustrate the particle morphology and widespread coalescence.

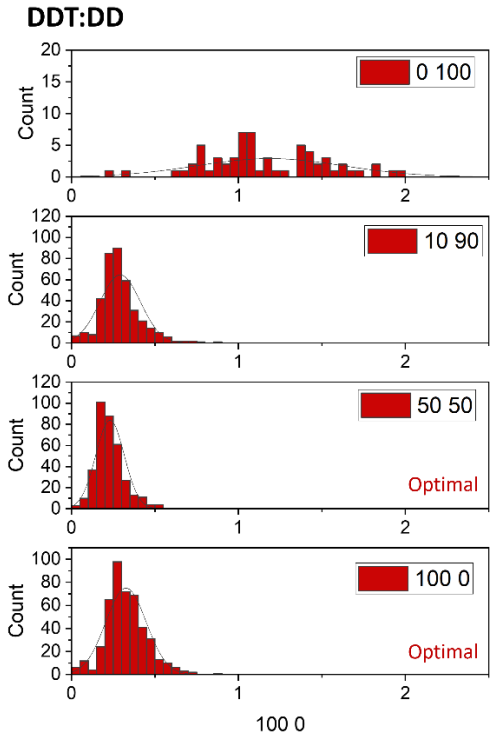

Supplementary Fig. 3 | Particle size distribution characterization under varying DDT:DD ratios. a, Particle Size Distribution Histogram. **b-d,** SEM Images of DDT:DD=10:90.

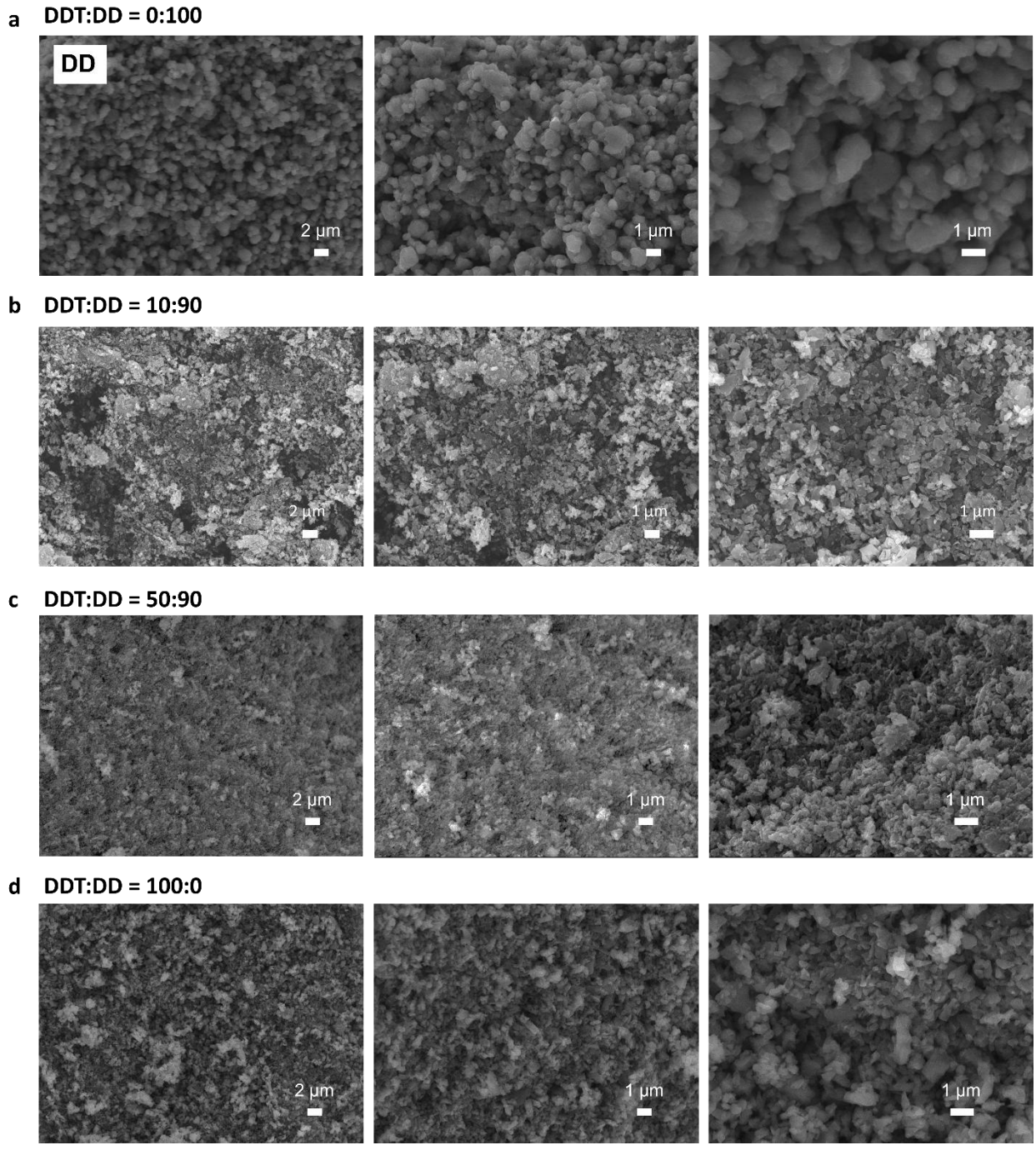

Supplementary Fig. 4 | Micromorphological (SEM) Characterization under varying DDT:DD ratios. Representative SEM micrographs of LPSCl particles milled with non-coordinating dodecane (DD) as a physical lubrication control, showcasing irregular particle shapes and insufficient refinement compared to the chemisorption-mediated strategy

Category	Milling condition	Before milling		After milling				Ref.
	Additive	Size (μm)	Ionic conductivity (mS cm^{-1})	Size (μm)	Ionic conductivity (mS cm^{-1})	Size / Ionic conductivity (μm cm mS^{-1})	Ionic conductivity loss rate (mS um^{-1} cm^{-1})%	
This work	DDT	100	5.12	0.4	2.69	6.725	2.440	
This work	DDT + DD	100	5.12	1	0.52	0.520	4.646	
1	-	11	3.08	2.42	0.57	0.236	29.254	1
2	-	11	3.08	2.44	0.44	0.180	30.841	1
3	-	11	3.08	2.6	0.39	0.150	32.024	1
4	Xylene	11	3.08	1.6	2.2	1.375	9.362	1
5	Xylene	11	3.08	0.9	1.9	2.111	11.683	1
6	Xylene	11	3.08	0.7	1.5	2.143	15.340	1
8	Xylene	10	3.2	4.5	1.8	0.400	25.455	2
9	Xylene	10.8	2.8	5.01	2.3	0.459	8.636	3
10	Xylene	10.8	2.8	1.54	1.8	1.169	10.799	3
11	Heptane		0.39	8	0.32	0.040		4
12	Heptane		0.39	5	0.24	0.048		4
13	Heptane + Dibutyl ether		0.39	3	0.22	0.073		4
14	Heptane + Dibutyl ether		0.39	1.5	0.14	0.093		4
15	-	35	3.99	12	2.8	0.233	5.174	5
16	-	35	3.99	1.1	0.6	0.545	10.000	5

Supplementary Table 1 | Comprehensive benchmarking of particle size and ionic conductivity across top-down refinement methods. Quantitative comparison of milling additives, particle sizes, room-temperature ionic conductivities, and conductivity decay rates Δσ/σ0) between this work and previously reported dry or wet ball-milling benchmarks.

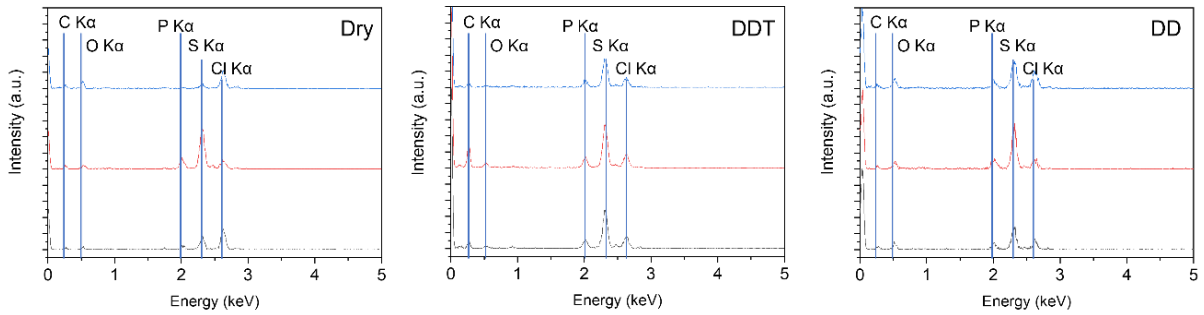

Supplementary Fig. 5 | Supplementary STEM-EDS spectral analysis under different milling conditions (Dry milling, DDT-assisted, and DD-assisted). In addition to the elemental mapping images, the point-analysis EDS spectra clearly confirm a localized increase in the Cl Kα peak intensity concurrent with a decrease in the S Kαpeak intensity within the clustered regions. Notably, C Kαand O Kαsignals are negligibly detected in the DDT-treated sample, verifying the highly preserved purity and effective removal of organic additives.

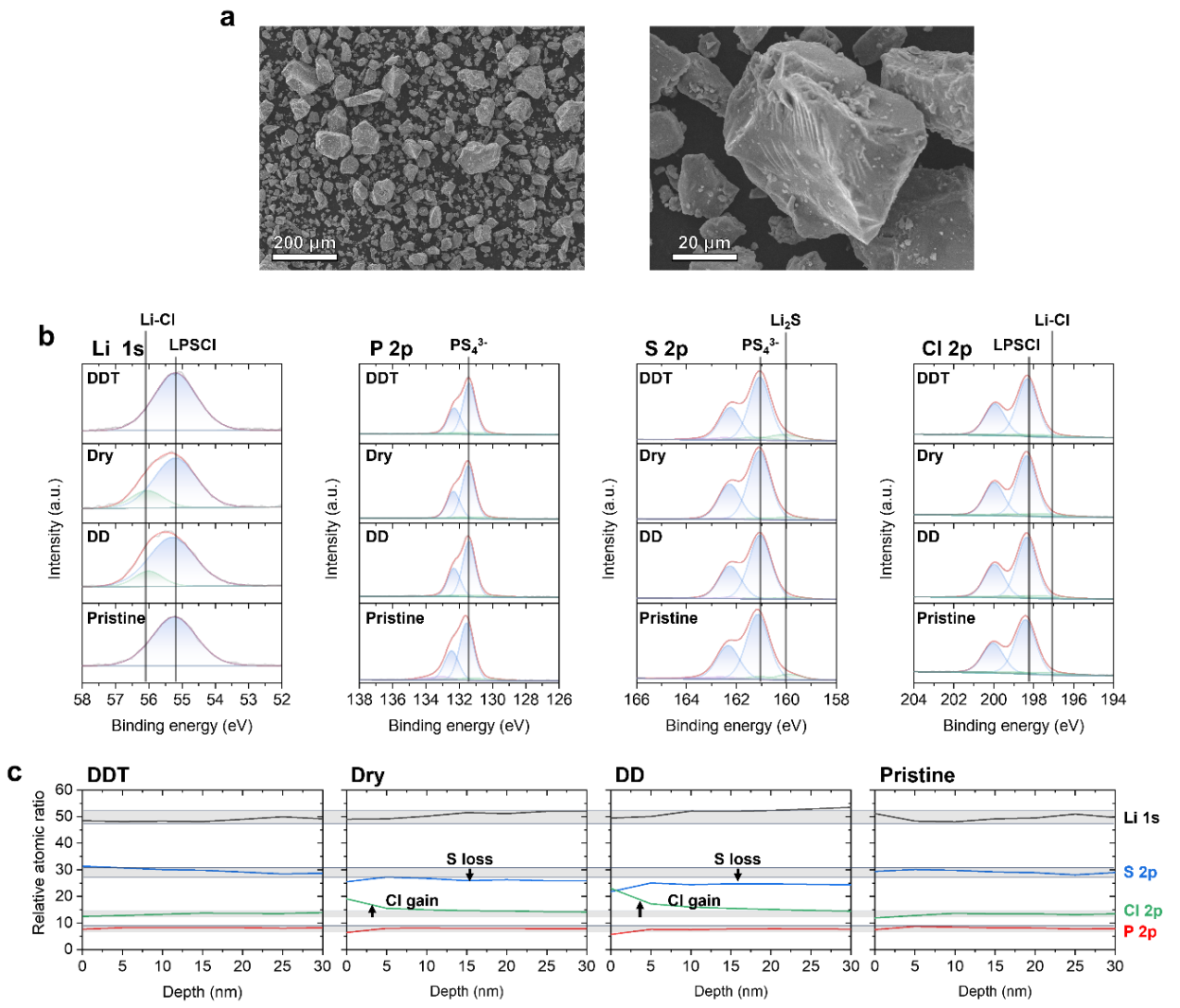

Supplementary Fig. 6 | Characterization of Pristine LPSCl and Comparative Analysis with Other Conditions. a, Scanning electron microscopy (SEM) images showing the surface morphology of as-received (pristine) LPSCl powder. The particles exhibit angular, crystalline shapes of various sizes, providing a morphological baseline for the material's initial state. Scale bars represent 200 µm and 20 µm, respectively. **b,** High-resolution Li 1s, P 2p, S 2p, and Cl 2p XPS spectra relative to the pristine baseline. The bottom row representing the pristine state serves as the reference standard for the treated groups (DDT, Dry, DD). The pristine spectra clearly define the primary chemical environments of the bulk material (e.g., peaks corresponding to PS_4^{3-} and Li-Cl). Notably, secondary phase impurity peaks such as Li_2S in the S 2p region, which are prominent in the Dry and DD conditions are virtually absent in the pristine sample. **c,** XPS depth profile analysis of pristine from 0 to 30 nm. The Pristine panel demonstrates a

uniform composition, where the relative atomic ratios of the four core elements (Li 1s, S 2p, Cl 2p, and P 2p) remain nearly constant throughout the sputtering depth. This presents a contrast to the Dry and DD conditions, which exhibit a distinct near-surface sulfur (S) loss and chlorine (Cl) gain. The DDT condition shows a trend highly similar to the pristine state.

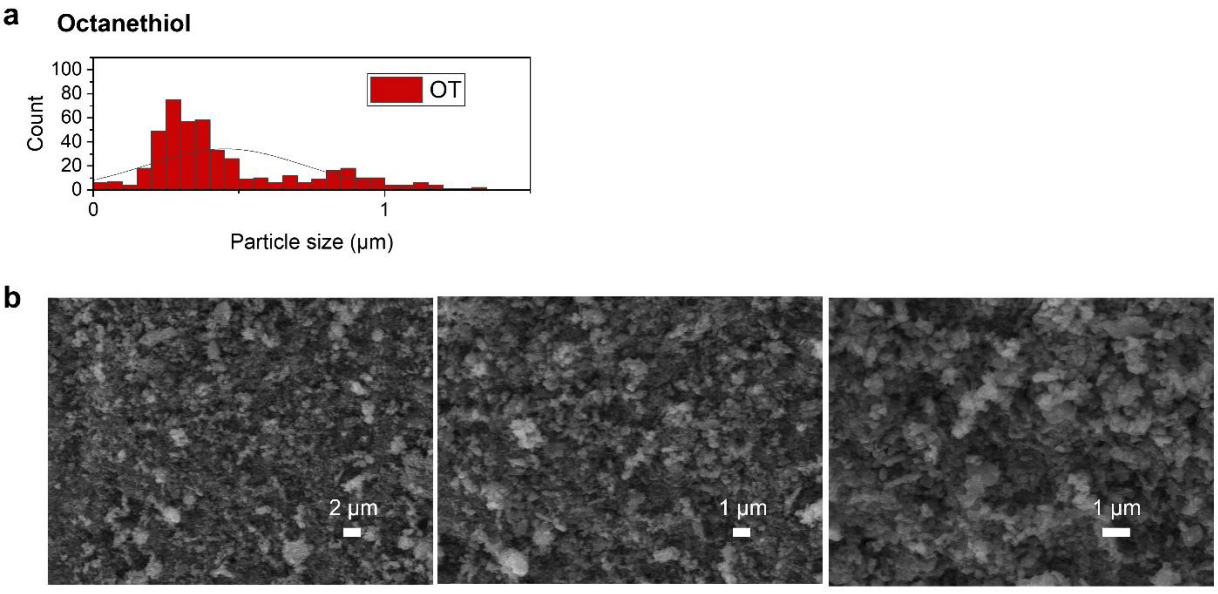

78

79 **Supplementary Fig. 7 | Particle Size Distribution and Morphological Characterization of**

80 **Octanethiol (OT) Samples. a,** Particle Size Distribution Histogram. **b,** SEM Images

81

82

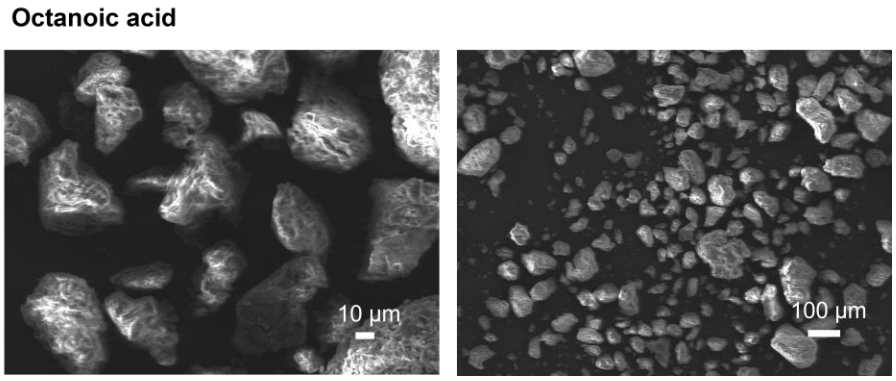

Supplementary Fig. 8 | SEM images of octanoic acid

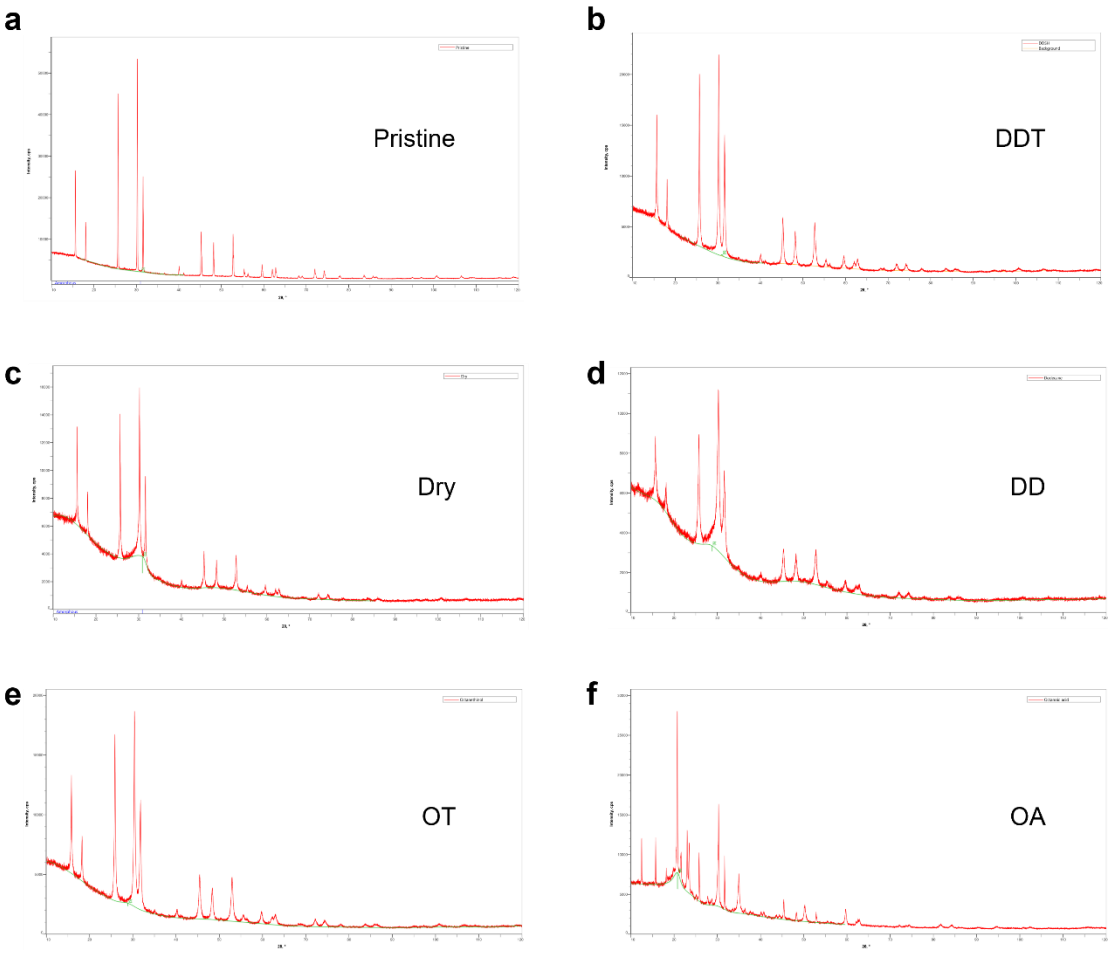

Supplementary Fig. 9 | Comparative XRD Analysis of the Solid Electrolyte under Various Chemical Treatment Conditions. The diffraction angle (θ) ranges from 10° to 120°, with the y-axis representing the diffraction intensity in counts per second. **a,** Pristine (As-Received State): a low background baseline with sharp, highly resolved diffraction peaks. This indicates excellent crystallinity and phase purity inherent to the initial material, establishing a reliable baseline for evaluating structural changes across other conditions. **b,** DDT (Dodecanethiol): well-Preserved Structure. This indicates that **DDT** effectively preserves the core crystalline framework of the solid electrolyte with minimal structural degradation, showing high chemical compatibility. **c-e,** Dry, DD (Dodecane), and OT (Octanethiol): a distinct, broad amorphous hump at lower angles (θ∼10° to 30°). This features suggests the development of surface structural disorder or the formation of amorphous secondary phases, although the primary bulk crystalline peaks remain intact. **f,** OA (Octanoic acid): a severe deviation from all other conditions. This provides clear

evidence of severe structural decomposition or the massive precipitation of a new secondary phase driven by the high chemical reactivity or acidity of octanoic acid.

Supplementary Note 1 | Effects of milling parameters on the size reduction behavior and ionic conductivity of solid electrolytes

Systematic evaluations were performed to investigate the impacts of various wet ball-milling parameters, including the concentration of dodecane thiol (DDT), solvent composition, milling duration, and rotational speed (RPM), on the minimum achievable particle size and corresponding ionic conductivity of argyrodite-type Li6PS5Cl solid electrolytes.

Concentration of DDT

The dosage of DDT serves as a critical lever for controlling the particle size distribution (PSD) while preserving the structural integrity of the crystalline electrolyte framework. Under the optimized weight ratio of DDT/Li_6PS_5Cl = 1.27, the system exhibits the narrowest PSD along with a minimized average particle size.

Conversely, an excessive introduction of liquid DDT does not significantly alter the minimum achievable particle size but leads to a substantial increase in the fraction of unrefined large particles. Mechanistically, an excess of liquid DDT reduces the statistical probability of solid particles being localized within the high-energy collision and shear zones at the ball–ball and ball–wall interfaces. Although the mechanical energy transferred per single impact remains identical, the cumulative exposure frequency diminishes. Consequently, this insufficient size reduction results in the coexistence of large particles that partially retain their pristine crystalline core (bulk-like core), which subsequently causes a slight increase in the overall ionic conductivity compared to the optimal condition.

On the other hand, deficient DDT ratios (e.g., 0.67) lead to a substantial increase in both the minimum and average particle sizes, accompanied by a severe degradation of ionic conductivity, mimicking the characteristics of dry milling. In this deficient state, the surface coverage of the liquid DDT is compromised, which simultaneously restricts both the structural preservation and mechanical refinement effects during the vigorous milling process.

Additive Composition (DDT:DD)

Interestingly, when DDT is blended with dichlorobenzene (DD) to reduce its concentration to 50% or 10%, a notable trend of decreased average particle size is observed compared to the pure DDT (100%) condition. This behavior is attributed to the viscosity difference between the two components ($\eta\_DD = 1.49$ mPa·s vs. $\eta\_DDT = 3.3$ mPa·s) as well as the surface anchoring effect of DDT. Compared to the single-component DDT system, the decreased viscosity in the binary mixture allows the effective grinding energy to be transferred more efficiently, while concurrently maintaining the intrinsic functionality of DDT[6]. Consequently, while employing 100% DDT as the baseline framework is reasonable when prioritizing structural stability and conductivity preservation, a 50:50 mixture condition offers a strategic alternative when ultra-fine particle control is the primary objective.

Milling Duration

The interplay between mechanical particle refinement and lattice defect accumulation is highly sensitive to the duration of the applied mechanical stress. During short-term milling (5 h and 10 h), the localized energy generated from individual impacts is sufficient to achieve a minimum particle size comparable to that of the optimal condition. However, due to the insufficient total exposure time in the high-shear zones[6], a large fraction of unrefined coarse particles remains, broadening the overall PSD. Because these large particles retain their inherent, pristine bulk-like cores, a relatively high ionic conductivity is preserved.

Extending the process to the optimal duration of 15 h ensures that the sample is exposed to the collision and shear zones with sufficient statistical frequency. This successfully establishes a highly uniform and narrow PSD while preventing severe structural degradation, thereby satisfying both target matrices. Beyond this optimal threshold, excessive milling for 20 h yields marginal further improvements in particle size reduction; instead, it triggers a precipitous decline in ionic conductivity. This degradation is ascribed to the progressive collapse of long-range and short-range structural ordering induced by the continuous accumulation of mechanical energy.

Mechanical Parameter: Rotational Speed (RPM)

With increasing rotational speed (RPM), which exhibits an effect analogous to extending the milling duration, the reduction in particle size was marginal, whereas a further degradation in ionic conductivity was observed. Therefore, considering the trade-off between particle size reduction efficiency and conductivity degradation, 500 RPM was selected as the optimal condition.

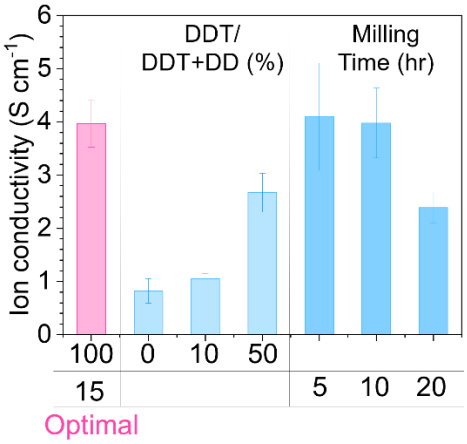

Supplementary Fig. 10 | Evaluation of optimization windows for wet ball-milling parameters. Plots tracking the average particle size and room-temperature ionic conductivity of LPSCl as a function of key processing variables: surfactant loading ratio DDT:LPSCl), binary mixture composition (DDT:DD ratio), mechanical milling duration 5h, 10hm 15h, and 20h), and rotational speed.

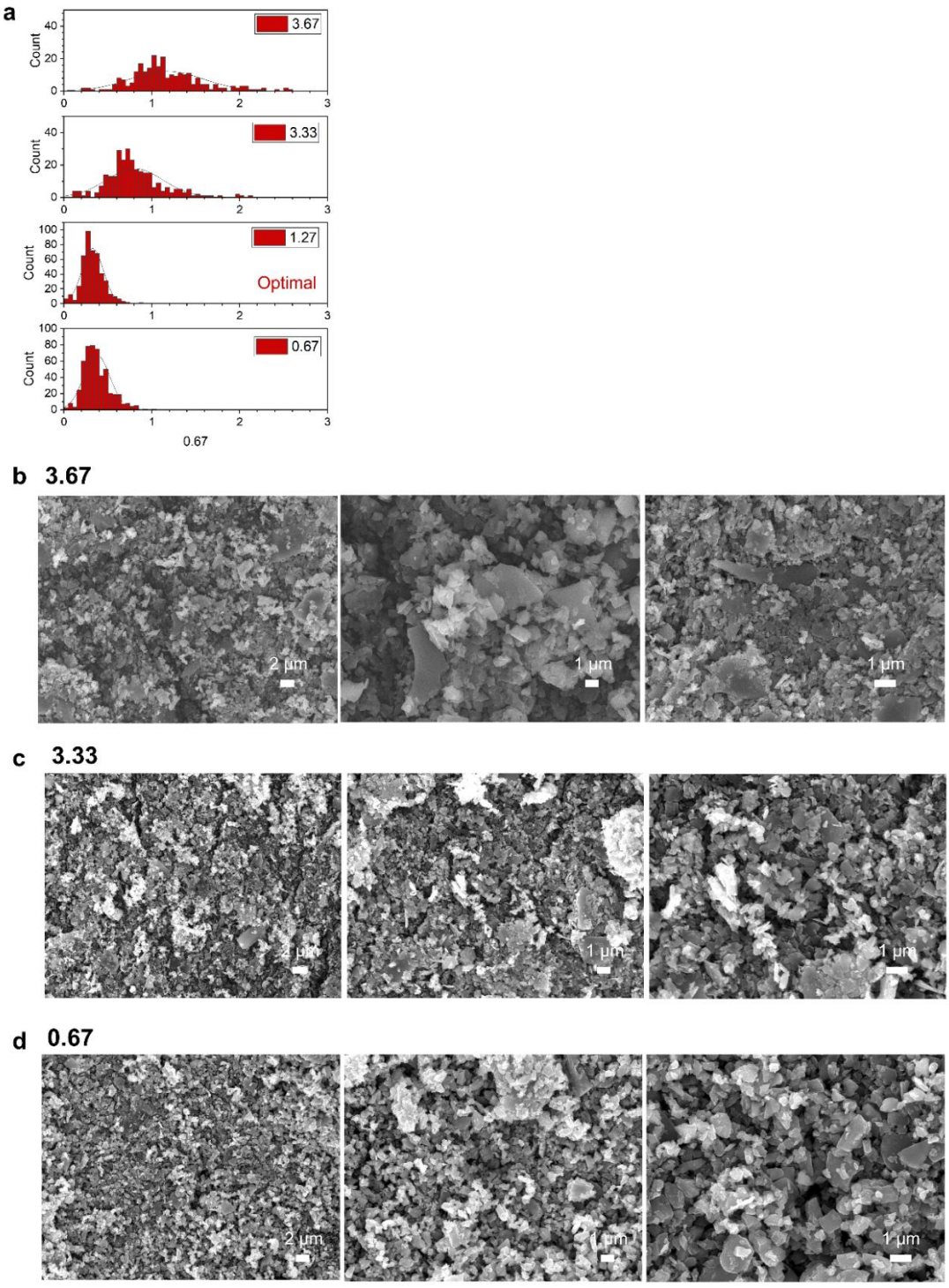

Supplementary Fig. 11 | Particle size distribution and micromorphological (SEM) characterization underv varying DDT/LPSCl ratios (3.67, 3.33, 1.27, and 0.67). a, Particle Size Distribution Histogram. **b-d,** SEM Images of 3.67(b), 3.33(c), and 0.67(d) DDT/LPSCl ratios.

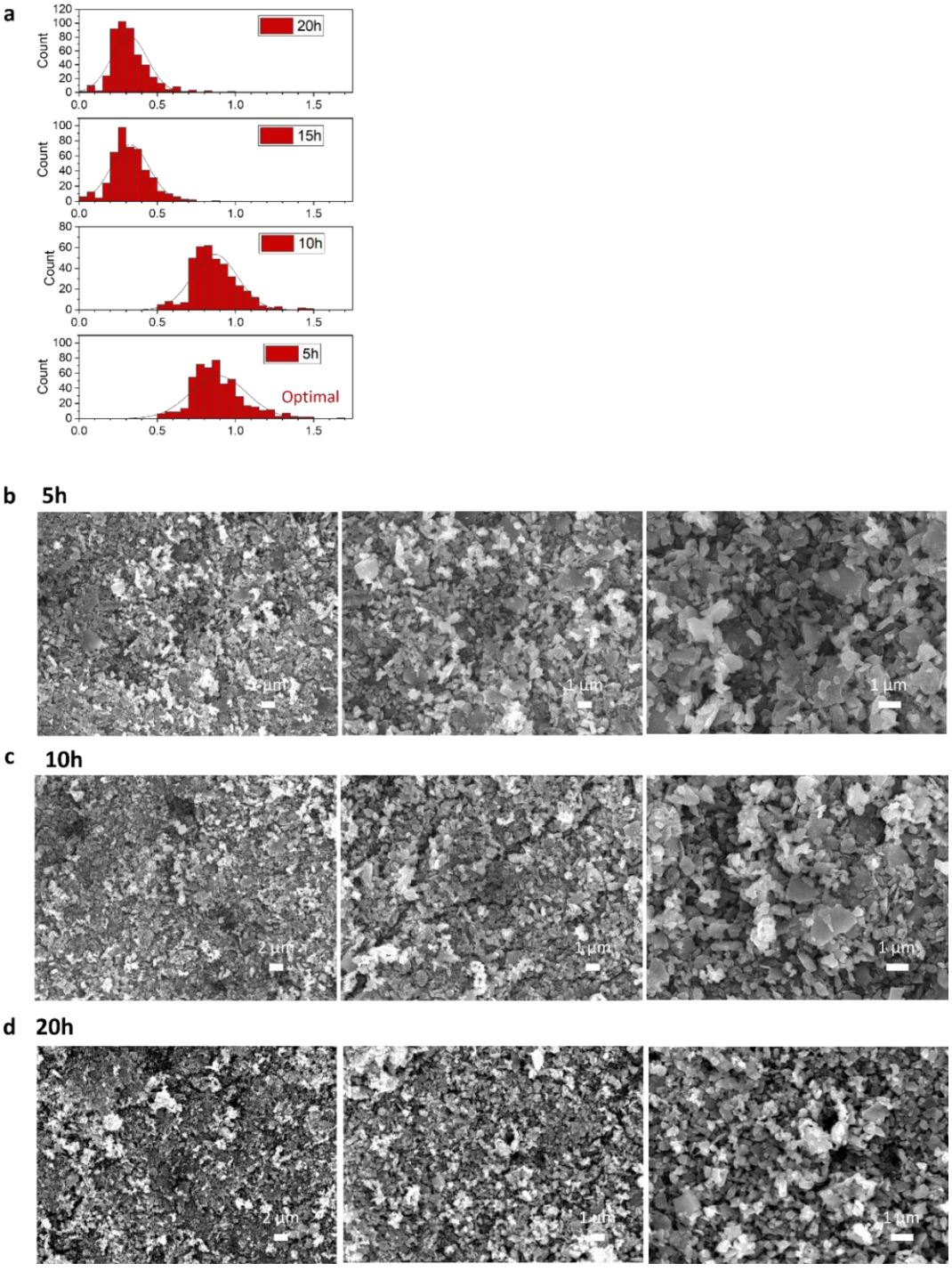

Supplementary Fig. 12 | Particle size distribution and micromorphological (SEM) characterization under varying milling time. a, Particle Size Distribution Histogram. **b-d,** SEM Images of 5h(b), 10h(c), and 20h(d).

Supplementary Fig. 13 | Digital photograph of a scalable slurry-cast solid electrolyte film. Visual presentation of a highly uniform, flexible, and macroscopic thin-film tape fabricated via doctor-blade casting using a printable slurry of SRMR-refined submicron solid electrolyte particles dispersed with a polymeric binder.

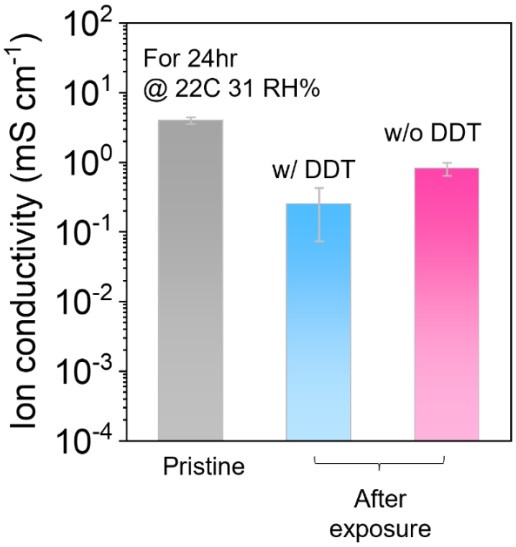

188

189 **Supplementary Fig. 14 | Ambient stability and moisture resistance evaluation.** Photographic
190 and structural comparison of pristine, bare, and DDT-passivated LPSCl powder beds before and
191 after exposure to an ambient atmosphere with controlled relative humidity 31%RH at 22°C for
192 24h, highlighting the hydrophobic shielding effect of the hydrocarbon chains.

193

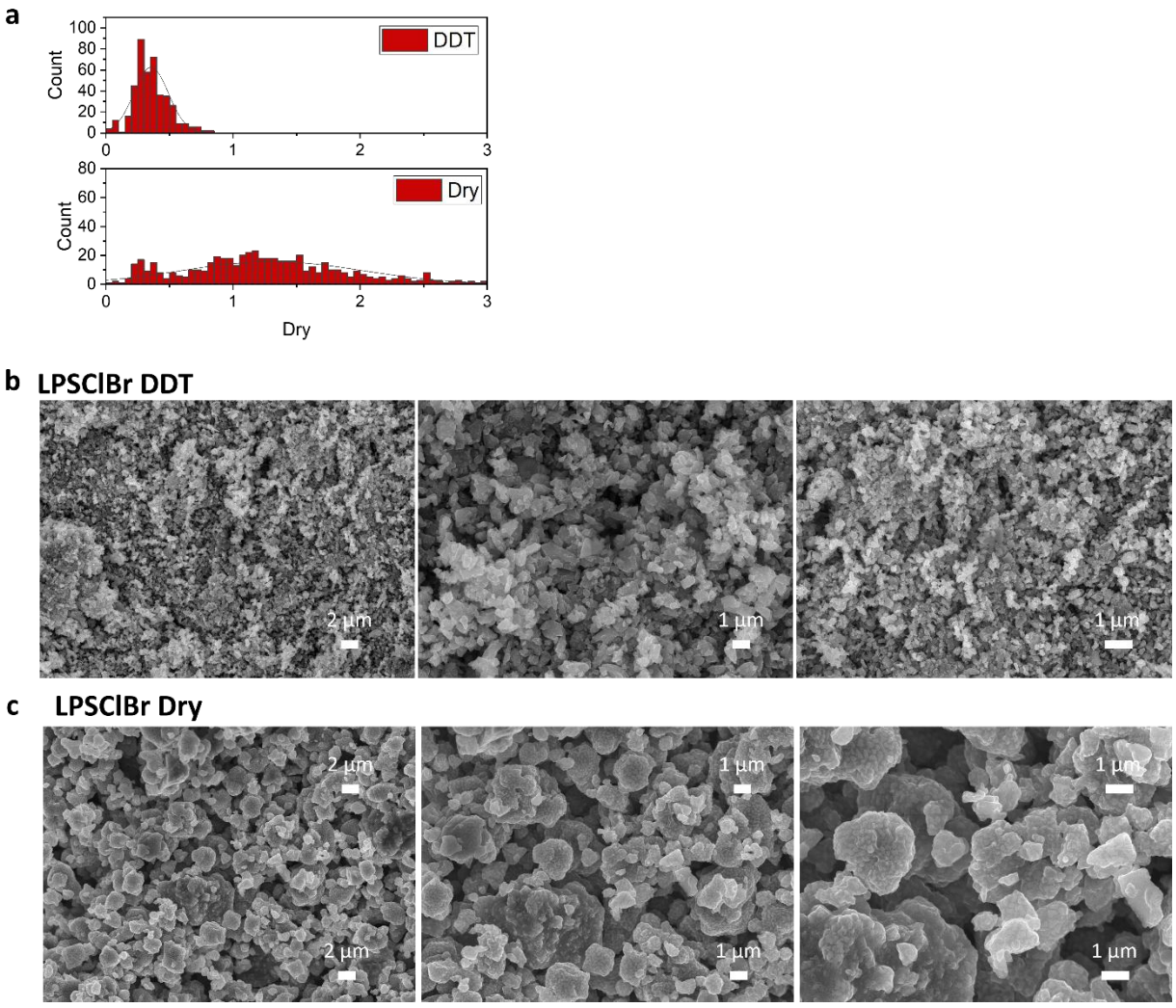

194

195 **Supplementary Fig. 15 | Particle size distribution and micromorphological (SEM)**
196 **characterization of LPSClBr. a,** Particle Size Distribution Histogram. **b-d,** SEM Images of
197 DDT-milled (b) and LPSClBr-milled (c) LPSCl.

198

Supplementary references

1. Tran, Q.-A. et al. Uni-Axial Densification of Slurry-Casted Li6PS5Cl Tapes: The Role of Particle Size Distribution and Densification Pressure. *Adv. Mater.* **37**, 2501592 (2025).

2. Kato, Y. et al. High-power all-solid-state batteries using sulfide superionic conductors. *Nat. Energy* **1**, 16030 (2016).

3. Wang, Y. et al. Mechanical Milling – Induced Microstructure Changes in Argyrodite LPSCl Solid-State Electrolyte Critically Affect Electrochemical Stability. *Adv. Energy Mater.* **14**, 2304530 (2024).

4. Shi, T. et al. High Active Material Loading in All-Solid-State Battery Electrode via Particle Size Optimization. *Adv. Energy Mater.* **9**, 1902881 (2019).

5. Kim, Y.-S. et al. Surficial Sulfur Loss of Jet-Milled Li6PS5Cl Powder under Mild-Temperature Heat Treatment. *ACS Appl. Energy Mater.* **5**, 15442–15451 (2022).

6. Patil, A. G. & Anandhan, S. Influence of planetary ball milling parameters on the mechano-chemical activation of fly ash. *Powder Technol.* **281**, 151–158 (2015).